

Dual channel CW nnU-Net for 3D PET-CT Lesion Segmentation in 2024 autoPET III Challenge

Ching-Wei Wang[✉], Ting-Sheng Su, and Keng-Wei Liu

Graduate Institute of Biomedical Engineering, National Taiwan University of Science and Technology, Taipei, Taiwan
cweiwang@mail.ntust.edu.tw

Abstract. PET/CT is extensively used in imaging malignant tumors because it highlights areas of increased glucose metabolism, indicative of cancerous activity. Accurate 3D lesion segmentation in PET/CT imaging is essential for effective oncological diagnostics and treatment planning. In this study, we developed an advanced 3D residual U-Net model for the Automated Lesion Segmentation in Whole-Body PET/CT - Multi-tracer Multicenter Generalization (autoPET III) Challenge, which will be held jointly with 2024 Medical Image Computing and Computer Assisted Intervention (MICCAI) conference at Marrakesh, Morocco. Proposed model incorporates a novel sample attention boosting technique to enhance segmentation performance by adjusting the contribution of challenging cases during training, improving generalization across FDG and PSMA tracers. The proposed model outperformed the challenge baseline model in the preliminary test set on the Grand Challenge platform, and our team is currently ranking in the 2nd place among 497 participants worldwide from 53 countries (accessed date: 2024/9/4), with Dice score of 0.8700, False Negative Volume of 19.3969 and False Positive Volume of 1.0857. GitHub repository is available at <https://github.com/cwwang1979/CW-nnU-Net-for-PET-CT>

Keywords: Deep Learning, whole-body PET/CT Imaging, Multi-tracer, 3D lesion segmentation, attention boosting.

1 Introduction

Oncological diagnostics have been significantly enhanced by Positron Emission Tomography / Computed Tomography (PET/CT) imaging, which provides essential insights necessary for accurate diagnosis and effective treatment planning[1,2]. Fluorodeoxyglucose (FDG) PET/CT is extensively used in imaging malignant tumors because it highlights areas of increased glucose metabolism, indicative of cancerous activity [3,4]. Besides FDG, prostate-specific membrane antigen (PSMA) is another crucial PET tracer used for the diagnosis and staging of prostate cancer, owing to its high expression on most prostate cancer cells [5,6].

A major barrier to clinical adoption of quantitative PET/CT analysis is lesion segmentation, a necessary step for detailed and individualized tumor characterization and therapeutic decision-making. Manual lesion segmentation is a labor-intensive and time-consuming process, making automated PET/CT lesion segmentation essential for enhancing efficiency, accuracy, and reproducibility.

Recent studies have demonstrated the potential of deep learning methods in the challenging task of automated PET/CT lesion segmentation, showing effective tumor segmentation across various research efforts. One approach derives attention maps from PET data to focus a convolutional neural network (CNN) on areas of the CT image with a higher likelihood of lung tumors [7]. Another method combines feature maps of different resolutions to create spatially varying fusion maps, enhancing lesion information for liver tumor segmentation [8]. Furthermore, promoting the segmentation of head and neck oropharyngeal primary tumors in FDG-PET/CT images, the HECKTOR challenge has shown that a 3D U-Net based approach significantly exceeded human inter-observer agreement levels, highlighting the effectiveness of automated segmentation methods [9].

The MICCAI 2024 Automated Lesion Segmentation in Whole-Body PET/CT - Multitracer Multicenter Generalization Challenge (autoPET III) [10], building upon the previous two challenges, i.e. 2022 autoPET and 2023 autoPET II, aims to meet the critical need for developing models capable of generalizing across various tracers and centers. The main objective is to accurately segment FDG- and PSMA-avid tumor lesions in whole-body PET/CT scans. The 2024 challenge provides FDG-PET/CT data from University Hospital Tübingen (UKT) and PSMA-PET/CT data from University Hospital LMU Munich (LMU), necessitating algorithms that minimize false-positive segmentation in anatomical structures with naturally high uptake. The complexity is heightened in a multi-tracer environment, as physiological uptake differs between tracers; for instance, FDG shows significant uptake in the brain, kidneys, and heart, whereas PSMA is more pronounced in the liver, kidneys, spleen, and submandibular glands.

In this study, we developed a 3D residual U-Net model with an enhanced architecture to increase depth and complexity, modifying both the encoder and decoder structures to improve feature extraction capabilities. Our training strategy incorporates a sample re-weighting technique, prioritizing more challenging samples to optimize model performance. Through iterative adjustments and re-training, this approach significantly improved segmentation accuracy and robustness.

2 Method

2.1 Data

The autoPET III challenge provides 1,611 studies in training dataset includes 1,014 FDG studies from 900 patients and 597 PSMA studies from 378 patients (see Table 1). The FDG group comprises 501 patients with histologically confirmed malignant melanoma, lymphoma, or lung cancer, along with 513 negative

control patients. The PSMA group consists of PET/CT images of 378 male individuals with prostate carcinoma, with 537 images showing PSMA-avid tumor lesions and 60 images without. The FDG dataset from UKT includes 570 male patients and 444 female patients. In contrast, the PSMA dataset from LMU consists of 378 male patients. Imaging conditions differ between the datasets; the FDG Tübingen dataset was obtained using a single Siemens Biograph mCT scanner, whereas the PSMA Munich dataset was collected using three different scanners: Siemens Biograph 64-4R TruePoint, Siemens Biograph mCT Flow 20, and GE Discovery 690 [11,12].

In the challenge preliminary evaluation, the test set is obtained from 5 studies in the released training dataset, includes 3 FDG studies and 2 PSMA studies. the final evaluation will be conducted using a hidden test set of 200 studies, comprising 50 FDG scans from LMU, 50 FDG scans from UKT, 50 PSMA scans from LMU, and 50 PSMA scans from UKT (see Table 1). Half of the test data will be drawn from the same sources and distributions as the training data, while the remaining half will be cross-sourced from the other center, ensuring a robust assessment of the model’s generalization capabilities. The FDG PET/CT training and testing images from UKT were annotated by a radiologist with a decade of experience in hybrid imaging, while those from LMU were annotated by a radiologist with eight years of experience. The PSMA PET/CT datasets from both centers were initially annotated by a single reader and subsequently reviewed by a radiologist with five years of experience in hybrid imaging.

Table 1. Materials: autoPET III Challenge Dataset.

Source Sites	Training (Public)	Validation (Public)	Testing (Private)
LMU Hospital	1014 studies (FDG)	3 studies (FDG)	50 studies (FDG)
			50 studies (PSMA)
UKT Hospital	597 studies (PSMA)	2 studies (PSMA)	50 studies (FDG)
			50 studies (PSMA)

In total, 1611 studies are released and made available for challenge participants, and we categorized the FDG and PSMA PET/CT images from both institutions into two categories: images with tumor annotations (positive diagnoses) and those without tumor annotations (negative studies). For model training and internal evaluation, only the annotated images were utilized, amounting to a total of 1,038 images, namely Dataset P (see Table 2).

Table 2. Categorization of Training Studies: Positive and Negative

All Training studies	Positive (Dataset P)	Negative (Non-utilized)
1611 studies	1038 studies	573 studies

2.2 Data Pre-processing

For data normalization, we firstly analyzed the intensity values from the foreground classes (excluding the background and ignore classes) from all training cases by computing the mean, standard deviation, and the 0.5 and 99.5 percentiles of these values. Intensity values were then clipped to the 0.5 and 99.5 percentiles, followed by subtraction of the mean and division by the standard deviation [13]. This data normalization was applied to each training case separately for individual input channels, namely CT and PET channels.

2.3 Data Augmentation

In the proposed framework, two data augmentation strategies were explored and tested initially, including Type1 and Type2 Augmentation.

Type1 Augmentation : The Type1 Augmentation includes basic transformations such as random rotation, cropping, scaling, Gaussian blur, Gaussian noise, contrast and brightness adjustments, down-sampling, and gamma correction. These augmentations are designed to enhance model robustness while maintaining the integrity of the original data distribution.

Type2 Augmentation : The Type2 Augmentation extends the Type1 strategy with more complex augmentations, including enhanced [scaling, contrast and brightness], sharpening, localized gamma transformations and random rectangle occlusion simulations. These aim to expose the model to a wider range of possible data variations.

Performance Comparison : By comparing the performance of Model2 and Model3, which are adopting Model1 as pre-trained weights, it is found that the Type1 Augmentation strategy outperforms Type2 Augmentation (see Table 3). While Type2 Augmentation provides a broader range of augmentations, it can introduce variations that deviate too far from the actual data, potentially leading to poor performance. In contrast, the Type1 strategy better preserves the original data characteristics, resulting in improved model performance. As a result, in the following models, we adopted the Type1 Augmentation strategy instead of Type2 Augmentation.

Table 3. Performance Comparison on Type1 and Type2 Augmentation

Model	Pre-trained weights	Data Augmentation	Dataset P (1038 files)		
			Dice score	False Positive Volume	False Negative Volume
Model1	-	Type1	0.8074	4.5071	6.3643
Model2	Model1	Type2	0.8048	4.8231	7.0752
Model3	Model1	Type1	0.8577	3.4134	5.1799

2.4 Model Architecture

Proposed model is built on a 3D residual U-Net architecture, manually adjusted to include a 7-stage encoder with convolutions arranged as (1,3,4,6,6,6,6). This enhances the model’s depth and complexity in the deeper stages. The decoder consists of 6 stages with one convolution per stage (1,1,1,1,1,1), designed to balance computational load while maintaining high performance. This setup deviates from the standard nnU-Net architecture, which typically includes a (1,3,4,6,6,6) encoder and a (1,1,1,1,1) decoder. Our modifications introduce an additional stage in both the encoder and decoder to create a deeper architecture.

The model processes 2-channel input data derived from CT and PET images. It utilizes a patch size of 128x256x256 and increases the maximum number of features from the standard limit of 320 to 384. This enhancement enables the model to capture more detailed features at deeper layers.

2.5 Training Strategy

Each model was trained with an initial learning rate of 0.0002. Additionally, we canceled the mirroring step in the data augmentation process, as the organs of the human body are not symmetrical. In our approach, we developed a sample attention boosting model, which emphasizing difficult samples during training. First, we randomly divided all positive studies in the training set, Dataset P (1038 samples), into Dataset A (934 samples) and Dataset B (104 samples) to evaluate model performance.

Table 4. Traininig Dataset Division

	Dataset P (1038 samples)			
	Dataset A (934 samples)		Dataset B (104 samples)	
Subset	Dataset A*	Dataset A**	Dataset B*	Dataset B**
Attribute	lower Dice score	remaining	lower Dice score	remaining
Number of samples	50	884	54	50

We used Dataset A as the training set to trained Model1 for 1500 epochs, resulting in a Dice score of 0.8074. By analyzing the Dice score of each sample from Model1 results, we further divided Dataset A and Dataset B as follows: Dataset A* with 50 samples and Dataset B* with 54 samples, both representing lower Dice samples, and Dataset A** with 884 samples and Dataset B** with 50 samples, both representing remaining samples (see Table 4). To improve the model’s accuracy, in Model2, we identified the 50 samples with lower Dice scores in Model1 and boosting the attention weights of these samples in the training set (see Table 5). Additionally, we added the 54 samples with lower Dice scores from Dataset B** into the training set. The aim was to increase the model attention onto the samples with poor prediction performance in the training set, with the

goal of improving performance. We subsequently employed Model1 as the pre-trained weights and re-trained it for 1000 epochs, while also modifying the data augmentation strategy from the Type1 to Type2 Augmentaion. However, the performance of Model2 did not improve significantly, with Dice score of 0.8048.

Table 5. Detail of training samples for each model.

Model	number of extra samples				samples from Dataset A	samples from Dataset B	total samples
	Dataset A*	Dataset A**	Dataset B*	Dataset B**			
Model1	0	0	0	0	934	0	934
Model2	50	0	0	0	934	54	1038
Model3	43	0	0	0	934	54	1031
Model4	43	17	5	0	934	104	1103
Model5	61	51	9	0	934	104	1159

In Model3, we did not boost sample attention weights of the samples with Dice score of 0. Instead, we boosted sample attention weights of 43 samples from Dataset A* and added 54 samples from Dataset B*. The Model1 was again used as a pre-trained weights, and the model was re-trained for 1000 epochs, achieving Dice score of 0.8577. In Model4, the Model4 training set continued from the Model3 training set. By evaluating the Dice scores of Model3 using Dataset A** and Dataset B*, we identified samples with Dice scores below 0.7: 17 samples from Dataset A** and 5 samples from Dataset B*. We further boosted sample attention weights of the identified samples in the training set. Additionally, we performed a continuous training based on Model3’s weights for 500 epochs, resulting in Dice score of 0.8715.

The Model5 training set continued from the Model4 training set. By evaluating the Dice scores of Model4 using Dataset A*, Dataset A** and Dataset B, we identified samples with Dice scores below 0.75: 18 samples from Dataset A*, 34 samples from Dataset A** and 4 samples from Dataset B. We had subsequently boosted sample attention weights of the identified samples in the training set. Furthermore, we performed a continuous training based on Model4’s weights for 500 epochs, resulting in Dice score of 0.8781.

2.6 Post-processing

No post-processing is performed for high computational efficiency.

3 Results

We evaluated the performance of our segmentation model using three evaluation metrics: the foreground Dice score, False Positive volume (FPvol) and False Negative volume (FNvol). The foreground Dice score evaluates the accuracy of the segmentation by quantifying the overlap between the predicted segmented lesions

and the actual lesions by manual annotations. The FPvol metric measures over-segmentation by determining the volume of incorrectly identified lesion regions that do not overlap with the reference annotations. In contrast, the FNvol metric gauges under-segmentation by calculating the volume of actual lesion regions that are not captured by the model’s segmentation, where these regions do not overlap with the predicted mask. These metrics provide a thorough evaluation of the model’s segmentation performance.

In Table 6, the performance metrics of Model1 on the Dataset P were as follows: Dice score of 0.8074, FNvol of 4.5071 and FPvol of 6.3643. Through series of optimizations from Model 1, 3, 4 to 5, including a sample attention boosting model, Type1 data augmentation and continuous training, we achieved significant improvements in Model5: Dice score of 0.8781, FNvol of 2.4250 and FPvol of 4.4920.

Table 6. Overall Model Performance

	Dataset A (934 samples)			Dataset B (104 samples)			Dataset P (1038 samples)		
	Dice	FPvol	FNvol	Dice	FPvol	FNvol	Dice	FPvol	FNvol
Model1	0.8229	4.6176	6.3638	0.6686	3.5148	6.3680	0.8074	4.5071	6.3643
Model2	0.8095	5.0585	7.2096	0.7621	2.7093	5.8679	0.8048	4.8231	7.0752
Model3	0.8607	3.6268	5.3192	0.8313	1.4965	3.9281	0.8577	3.4134	5.1799
Model4	0.8718	3.2122	5.0088	0.8690	1.1432	3.3856	0.8715	3.0049	4.8462
Model5	0.8779	2.6001	4.6241	0.8801	0.8521	3.3054	0.8781	2.4250	4.4920

In Tables 7 and 8, the Dice scores of Model1 with evaluation using Dataset A*, i.e. samples with the lower Dice score, and using Dataset B* were 0.3261 and 0.4967, respectively. By boosting the attention weights of the samples with the lower Dice scores by the preliminary model, the model was better trained by putting extra focus on poorly segmented cases, thereby improving overall performance. Consequently, the Dice scores of Model5 evaluated on samples with lower Dice scores by the previous Model improved significantly, i.e. from 0.3261 to 0.6485 for Dataset A* and from 0.4967 to 0.8471 for Dataset B*.

Table 7. Quantitative Result of samples with lower Dice (A*) and remaining samples (A**)

	Dataset A					
	Dataset A* (lower Dice 50 samples)			Dataset A** (remaining 884 samples)		
	Dice	FPvol	FNvol	Dice	FPvol	FNvol
Model1	0.3261	31.3092	49.7958	0.8510	3.1079	3.9073
Model2	0.4155	29.4534	50.2960	0.8318	3.6797	4.7726
Model3	0.5721	24.3287	39.1188	0.8770	2.4559	3.4075
Model4	0.6319	22.9165	36.9530	0.8853	2.0960	3.2020
Model5	0.6485	17.8155	30.5988	0.8908	1.7395	3.1550

Table 8. Quantitative Result of samples with lower Dice (B*) and remaining samples (B**)

	Dataset B					
	Dataset B* (lower Dice 54 samples)			Dataset B** (remaining 50 samples)		
	Dice	FPvol	FNvol	Dice	FPvol	FNvol
Model1	0.4967	3.7272	9.9517	0.8542	3.2854	2.4976
Model2	0.6939	2.7421	8.9123	0.8357	2.6739	2.5800
Model3	1.0561	5.2380	12.5645	0.8792	3.5535	2.5135
Model4	1.0111	3.8111	4.4965	0.8965	1.2860	1.7538
Model5	0.8471	0.8636	4.7301	0.9157	0.8398	1.7667

In Table 9, the **datacentric_baseline** refers to the official baseline model provided by the autoPET III challenge organizers, as listed in the preliminary test set leader board on the Grand Challenge platform. Our initial Model1, trained on the partial positive training dataset A, obtained Dice score of 0.8402, FNvol of 26.2889 and FPvol of 1.4888. Through the proposed attention boosting method and continuous training strategy, a significant improvement is observed in Model5, achieving Dice score of 0.8700, FNvol of 19.3969 and FPvol of 1.0857. Our team is currently ranking in the 2nd place among 497 participants worldwide from 53 countries (accessed date: 2024/9/4).

Table 9. Preliminary Test Set Result in the Leader board (accessed date: 2024/9/4)

Rank	Model	Dice score	False Negative Volume	False Positive Volume
3rd	Model5	0.8700	19.3966	1.0857
4th	Model4	0.8632	20.4623	1.0334
7th	Model3	0.8462	21.1228	1.6206
9th	Model1	0.8402	26.2889	1.4888
15th	datacentric_baseline	0.7990	23.8380	2.0503

Figure 1,2,3 present the whole-body lesion segmentation results using CT and PET images generated by the proposed method, accompanied by a qualitative analysis comparing the predicted segmentations with the ground truth annotations. Through qualitative analysis, it can be observed that the predicted results demonstrate a high level of consistency with the ground truth in terms of lesion segmentation, indicating good model performance. Particularly in lesion boundary and region identification, the predicted segmentation outcomes closely match the manual annotation results.

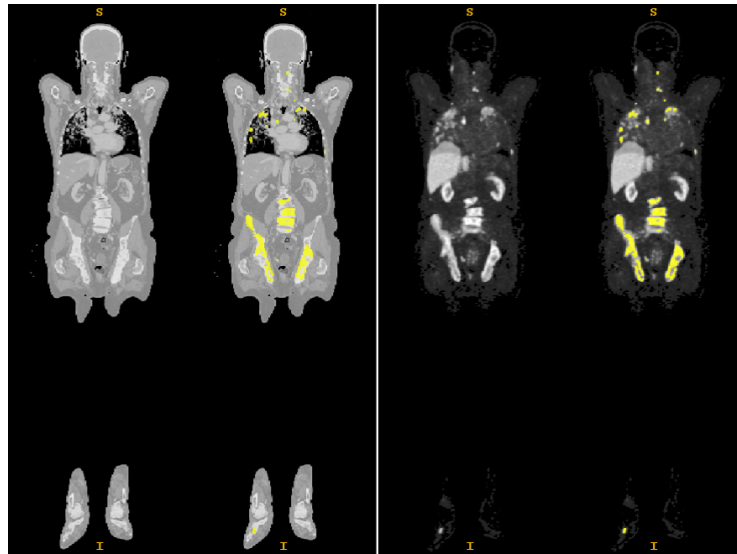


Fig. 1. Qualitative whole-body lesion segmentation results using CT and PET Images CT (left) and PET (right) with yellow segmentation masks

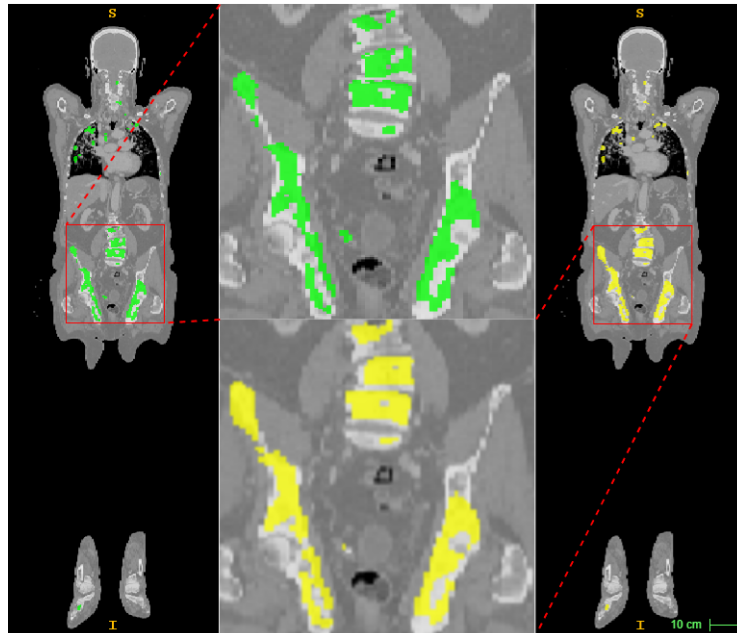


Fig. 2. Whole-body lesion segmentation results on CT images. The left side displays the manually annotated ground truth lesions (in green), while the right side shows the predicted segmentation results from the model (in yellow). The middle section provides a zoomed-in view of the lesion areas.

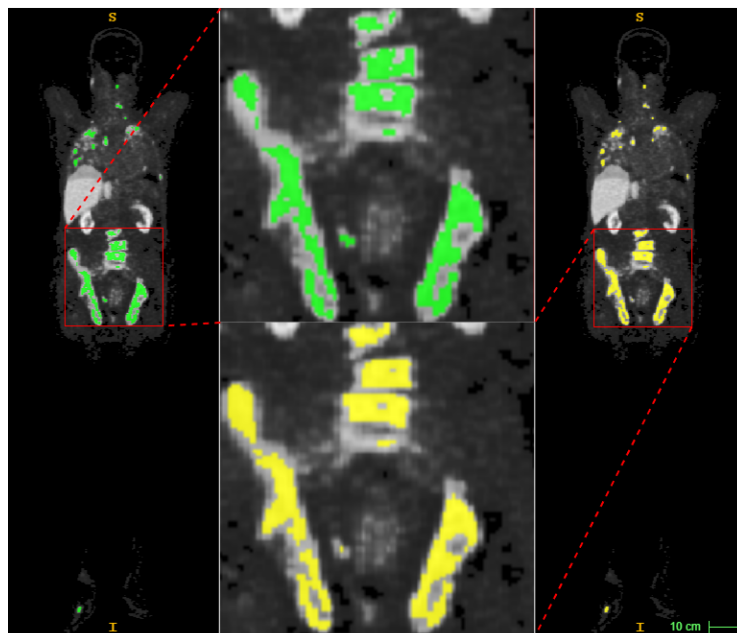


Fig. 3. Whole-body lesion segmentation results on PET images. The left side displays the manually annotated ground truth lesions (in green), while the right side shows the predicted segmentation results from the model (in yellow). The middle section provides a zoomed-in view of the lesion areas.

4 Discussion

To address the challenge of PET/CT data from multiple tracers and centers, we proposed a dual channel CW nnU-Net with a sample attention boosting model, achieving low FPvol, low FNvol and high Dice score. This technique emphasizes difficult samples during training, adjusting their contribution to improve the model's performance. The results from the preliminary test set on the Grand Challenge platform demonstrated the effectiveness of the proposed training strategy (see Table 9).

5 Acknowledgement

This study is supported by the National Science and Technology Council of Taiwan (NSTC 113-2222-E-011-003-MY3).

References

1. Li, R., Ravizzini, G.C., Gorin, M.A., Maurer, T., Eiber, M., Cooperberg, M.R., Alemozzaffar, M., Tollefson, M.K., Delacroix, S.E., Chapin, B.F.: The use of pet/ct in prostate cancer. *Prostate cancer and prostatic diseases* **21**(1), 4–21 (2018)
2. Lang, D., Wahl, G., Poier, N., Graf, S., Kiesl, D., Lamprecht, B., Gabriel, M.: Impact of pet/ct for assessing response to immunotherapy—a clinical perspective. *Journal of Clinical Medicine* **9**(11), 3483 (2020)
3. Hirata, K., Tamaki, N.: Quantitative fdg pet assessment for oncology therapy. *Cancers* **13**(4), 869 (2021)
4. Parihar, A.S., Dehdashti, F., Wahl, R.L.: Fdg pet/ct-based response assessment in malignancies. *Radiographics* **43**(4), e220122 (2023)
5. Farolfi, A., Calderoni, L., Mattana, F., Mei, R., Telo, S., Fanti, S., Castellucci, P.: Current and emerging clinical applications of psma pet diagnostic imaging for prostate cancer. *Journal of Nuclear Medicine* **62**(5), 596–604 (2021)
6. Combes, A.D., Palma, C.A., Calopedos, R., Wen, L., Woo, H., Fulham, M., Leslie, S.: Psma pet-ct in the diagnosis and staging of prostate cancer. *Diagnostics* **12**(11), 2594 (2022)
7. Fu, X., Bi, L., Kumar, A., Fulham, M., Kim, J.: Multimodal spatial attention module for targeting multimodal pet-ct lung tumor segmentation. *IEEE Journal of Biomedical and Health Informatics* **25**(9), 3507–3516 (2021)
8. Xue, Z., Li, P., Zhang, L., Lu, X., Zhu, G., Shen, P., Shah, S.A.A., Bennamoun, M.: Multi-modal co-learning for liver lesion segmentation on pet-ct images. *IEEE Transactions on Medical Imaging* **40**(12), 3531–3542 (2021)
9. Oreiller, V., Andrearczyk, V., Jreige, M., Boughdad, S., Elhalawani, H., Castelli, J., Vallières, M., Zhu, S., Xie, J., Peng, Y., et al.: Head and neck tumor segmentation in pet/ct: the hecktor challenge. *Medical image analysis* **77**, 102336 (2022)
10. Ingrisch, M., Dexl, J., Jeblick, K., Cyran, C., Gatidis, S., Kuestner, T.: Automated Lesion Segmentation in Whole-Body PET/CT - Multitracer Multicenter generalization (Apr 2024). <https://doi.org/10.5281/zenodo.10990932>
11. Gatidis, S., Kuestner, T.: A whole-body fdg-pet/ct dataset with manually annotated tumor lesions (fdg-pet-ct-lesions) [dataset] (2022). <https://doi.org/10.7937/gkr0-xv29>

12. Gatidis, S., Kuestner, T.: A whole-body psma-pet/ct dataset with manually annotated tumor lesions (psma-pet-ct-lesions) (version 1) [dataset] (2024). <https://doi.org/10.7937/r7ep-3x37>
13. Isensee, F., Jaeger, P.F., Kohl, S.A., Petersen, J., Maier-Hein, K.H.: nnu-net: a self-configuring method for deep learning-based biomedical image segmentation. *Nature methods* **18**(2), 203–211 (2021)